Chapter 5
The Hamada Spectrum and Hamada Basis Vectors in HSX

5.0 Introduction

As will be made clear in the next chapter, it is necessary to describe the geometry of HSX in the Hamada coordinate system. The magnetic field must be Fourier decomposed in this coordinate system, and the basis vectors must be calculated. Further, flux surface averaged quantities such as $\langle \mathbf{B}_P \cdot \mathbf{B}_P \rangle$ and $\langle \mathbf{B}_T \cdot \mathbf{B}_T \rangle$ must be calculated for the actual geometry of HSX. The analytic and numerical techniques used for these calculations are described in this chapter, and the results will be used extensively in the modeling described in the next chapter.

Section 1 of this chapter comprises a brief review of flux coordinates. Section 2 describes how the spectrum of |B| is calculated by field line following, for either the Boozer or Hamada coordinate systems. Simple comparisons between the Boozer and Hamada spectra are provided. Section 3 illustrates the Hamada spectra for some interesting HSX configurations. Section 4 will present the details of the method for calculating the basis vectors. Section 5 will compare these numerical results with the large aspect ratio tokamak approximation.

5.1 Flux Coordinates and the Hamada Coordinate System

The modeling discussed in the next two chapters will make extensive use of flux coordinates, and the Hamada coordinate system in particular. Hence, a brief introduction to these coordinate systems is appropriate before discussing the physics. A very thorough discussion of vector and tensor calculus, magnetic flux coordinates, and Hamada coordinates in general can be found in the book by D'haeseleer.[1]

Throughout this work, the Hamada toroidal and poloidal angles will be called α and ζ respectively. A general flux surface label ρ will be used for theoretical discussion, although the

toroidal flux will be used as the flux label for numerical calculations. Cyclic order in these variables will be (ρ,ζ,α), and the angle variables will vary from 0 to 2π.

As a vector in a curvilinear coordinate system, the magnetic field (or any other vector) can be expressed as

$$\mathbf{B} = B^{\zeta}\mathbf{e}_{\zeta} + B^{\alpha}\mathbf{e}_{\alpha} + B^{\rho}\mathbf{e}_{\rho}, \tag{5.1}$$

with $B^{\alpha}=B\cdot\nabla\alpha$, $B^{\zeta}=B\cdot\nabla\zeta$, and $B^{\rho}=B\cdot\nabla\rho$, or as

$$\mathbf{B} = B_{\zeta}\nabla\zeta + B_{\alpha}\nabla\alpha + B_{\rho}\nabla\rho, \tag{5.2}$$

with $B_{\zeta}=\mathbf{B}\cdot\mathbf{e}_{\zeta}$, $B_{\alpha}=\mathbf{B}\cdot\mathbf{e}_{\alpha}$, $B_{\rho}=\mathbf{B}\cdot\mathbf{e}_{\rho}$. With the Jacobian written as

$$\sqrt{g} = \left(\nabla\rho\cdot\left(\nabla\zeta\times\nabla\alpha\right)\right)^{-1}, \tag{5.3}$$

the relationship between the covariant and contravariant basis vectors can be written as:

$$\mathbf{e}_{i} = \sqrt{g}\left(\nabla u^{j}\times\nabla u^{k}\right), \tag{5.4}$$

$$\nabla u^{i} = \frac{1}{\sqrt{g}}\left(\mathbf{e}_{j}\times\mathbf{e}_{k}\right), \tag{5.5}$$

with {i,j,k} representing cyclic order in the variables.

In the situations of interest in this work, the magnetic field lines form flux surfaces, so that $B^{\rho}=0$. Under these conditions and with $\nabla\cdot\mathbf{B}=0$, it can be shown that the contravariant field components can be written as

$$B^{\zeta} = \frac{1}{2\pi\sqrt{g}}\frac{\partial\psi_{tor}}{\partial\rho}, \tag{5.6}$$

$$B^{\alpha} = \frac{1}{2\pi\sqrt{g}}\frac{\partial\psi^{r}_{pol}}{\partial\rho}. \tag{5.7}$$

Here, ψ_{tor} is the toroidal flux through a surface and ψ^{r}_{pol} is the poloidal ribbon flux; these quantities are related to each other through the rotational transform

$$\iota = \frac{\partial \psi^{r}_{pol}}{\partial \rho} \Big/ \frac{\partial \psi_{tor}}{\partial \rho}. \tag{5.8}$$

Hence, the ratio of B^{ζ} to B^{α} is a constant, and the field lines are straight in this coordinate system.

The angles α and ζ can be modified to allow further choices of properties while maintaining the property of straight field lines. It is this second degree of freedom which makes the difference between Boozer coordinates, Hamada coordinates, or any other set of magnetic coordinates. In particular, Hamada coordinates are chosen so that the equilibrium currents as well as the magnetic field lines are straight lines in α and ζ. This choice leads to a Jacobian of the form

$$\sqrt{g}_{H} = \frac{1}{4\pi^2}\frac{dV}{d\rho}, \tag{5.9}$$

where V is the volume. In Section 5.4.4 on the calculation of the Pfirsch-Schlueter currents, it will be shown in detail that this choice of Jacobian leads to straight current lines. A different choice is made in Boozer coordinates (the periodic part of the scalar magnetic potential vanished in Boozer coordinates, see discussion by D'haeseleer), leading to a Jacobian of the form

$$\sqrt{g}_{B} = \frac{\mu_o}{(2\pi)^2}\frac{\iota I_{tor} + I^{d}_{pol}}{B^2}. \tag{5.10}$$

Here, I_{tor} is the total toroidal current enclosed by the surface, and I^{d}_{pol} is the poloidal disk current outside the surface of interest (equal to the sum of all magnet currents for HSX).

There will often be a need to take flux surface average of quantities. This average is the average of some quantity F(**R**) over the small volume between surfaces at ρ and $\rho+\Delta\rho$

$$\langle F(R) \rangle = \lim_{\Delta V \to 0} \frac{\iiint_{\Delta V} F(\vec{R})\, dV}{\iiint_{\Delta V} dV}. \tag{5.11}$$

It can be shown that for an arbitrary toroidal system, this expression reduces to

$$\langle F(\mathbf{R})\rangle = \frac{\int_0^{2\pi}\int_0^{2\pi} F(\mathbf{R})\sqrt{g}\,d\zeta\,d\alpha}{\int_0^{2\pi}\int_0^{2\pi}\sqrt{g}\,d\zeta\,d\alpha}. \tag{5.12}$$

In Hamada coordinates, the Jacobian is a flux surface quantity and can be factored out of both integrals, yielding simply

$$\langle F(\mathbf{R})\rangle = \frac{1}{2\pi}\int_0^{2\pi}\int_0^{2\pi} F(\mathbf{R})\,d\zeta\,d\alpha. \tag{5.13}$$

5.2 Calculation of the Hamada and Boozer Spectrum.

As will be shown in Chapter 6, the Hamada spectrum is an important component of the damping calculation. The method for numerical calculation of the Boozer spectrum was first reported by Kuo-Petravic[2] et al., and modified by Talmadge[3] for the calculation of the Hamada spectrum. This method is briefly recounted below, and notes about the numerical implementation of the algorithm are provided where necessary.

All calculations from this point forward are in the mks system of units. The toroidal flux ψ, with units of Tm^2 will be used as the surface label. Cyclic order in the flux coordinate variables will be (ρ,ζ,α), while cyclic order in the lab coordinate system will be (R,Φ,Z).

The contravariant components of the field are defined in terms of the Jacobian

$$\mathbf{B}\cdot\nabla\zeta = \frac{1}{2\pi\sqrt{g}}, \tag{5.14}$$

$$\mathbf{B}\cdot\nabla\alpha = \frac{\iota}{2\pi\sqrt{g}}. \tag{5.15}$$

These expressions can be integrated to solve for the angles themselves as

$$\zeta = \int \frac{dl}{B} \frac{1}{2\pi\sqrt{g}}, \tag{5.16}$$

$$\alpha = \int \frac{dl}{B} \frac{\iota}{2\pi\sqrt{g}}. \tag{5.17}$$

Recall that the magnetic field is expanded in Fourier harmonics as

$$B = B_o \sum_{n,m} b_{nm} \cos(n\zeta - m\alpha). \tag{5.18}$$

By substituting (5.16) and (5.17) into (5.18), it is possible to show that

$$B = B_o \sum_{n,m} b_{nm} \cos\left(\frac{(n - m\iota)}{2\pi} \int \frac{dl}{B\sqrt{g}} \right). \tag{5.19}$$

Recall that the Jacobian in Hamada and Boozer coordinates is given by

$$\sqrt{g}_H = \frac{1}{(2\pi)^2} \frac{dV}{d\psi}, \tag{5.20}$$

$$\sqrt{g}_B = \frac{\mu_o}{(2\pi)^2} \frac{\iota I_{tor} + I_{pol}^d}{B^2}. \tag{5.21}$$

Using these Jacobians, the Fourier expansion can be written as

$$B(\chi) = B_o \sum_{n,m} b_{nm} \cos(\omega_{nm} \chi(l)). \tag{5.22}$$

For the Hamada spectrum, ω_{nm} and χ are given by

$$\omega_{nm,H} = \frac{(n - m\iota)2\pi}{dV/d\psi}, \tag{5.21}$$

$$\chi_H(l) = \int^l \frac{dl}{B}. \tag{5.22}$$

For the Boozer spectrum, under the assumption of no net toroidal current, ω_{nm} and χ are given by

$$\omega_{nm,B} = \frac{(n - m\iota)}{\pi g_B}, \tag{5.23}$$

$$\chi_B(l) = \int^{l} B\,dl, \tag{5.24}$$

where $g_B=(\mu_o/2\pi^2)\Sigma(I_P)$. As an example, for the standard QHS configuration of HSX, $g_B=2\cdot10^{-7}\cdot$(14 turns)$\cdot$(48 coils)$\cdot$5361 Amps=0.7205. This number can also be found by calculating one toroidal transit of the $\int\mathbf{B}\cdot d\mathbf{l}$ integral along the magnetic axis.

In the implementation of the algorithm, the field line is integrated forward in equal increments of χ. This is done in the Hamada case by solving the following equations to integrate the trajectory of the field line:

$$dR/d\chi_H = B_R, \tag{5.25a}$$

$$d\Phi/d\chi_H = B_\Phi/R, \tag{5.25b}$$

$$dZ/d\chi_H = B_Z. \tag{5.25c}$$

The integration is typically done for 2^{17} points equally spaced from $\chi_H=0$ to $\chi_H=2800$, although it is sometimes necessary to integrate further if the surface shape is complicated, as near a magnetic island. The MATLAB ODE113 (variable order Adams-Bashforth-Moulton method) integrator is used, with an absolute tolerance of 10^{-10} and a relative tolerance of 10^{-8}. As a part of this calculation, the Hamada Jacobian is calculated by recalling that

$$\frac{dV}{d\psi} = \frac{1}{N}\int^{l}\frac{dl}{B}, \tag{5.26}$$

where N is the number of toroidal transits made in the integration.

For the Boozer spectrum, the integration in equally spaced increments in χ is done by integrating the equations

$$dR/d\chi_B = B_R/B^2, \tag{5.27a}$$

$$d\Phi/d\chi_B = B_\Phi/RB^2, \tag{5.27b}$$

$$dZ/d\chi_B = B_Z/B^2. \tag{5.27c}$$

The integration is typically done for 65536 points equally spaced from χ_B=0 to χ_B=300. As with the Hamada case, integrating further in χ may be necessary depending on the magnetic surface. In all cases, it is necessary to integrate in small enough steps that small variations in B (like modular coil ripple) can be clearly resolved. At the end of this step, a full B vs. χ curve has been calculated.

In order to calculate b_{nm} and as well as the associated n and m, it is necessary to take the FFT of B(χ), leading to FB(ω). A Gaussian window function is typically applied to the data before taking the FFT. This quantity FB(ω) will have many peaks, with each peak corresponding to a specific spectral component. The ω axis can be converted to an n-mι axis using the relationships in (10) or (12). Note that integrating farther in χ will lead to more dense point spacing in the (n-mι) axis, while integrating at finer spaced points on the B vs. χ curve leads to the ability to resolve spectral components at higher values of n-mι.

The final step in the spectrum calculation is to find the peaks in FB(n-mι) and allocate n and m numbers. An initial sweep over the data finds the locations of the peaks, while a second step fits Gaussians to the peaks to accurately locate them in n-mι. The height of the peaks is the coefficient b_{nm}. Knowing ι, it is then possible to allocate n and m numbers to the peaks, completing the calculation.

As a check on the quality of the calculation, the numerically integrated B vs. χ curve can be compared with the curve calculated from the spectrum using equation 5.19. An example of this comparison can be seen in figure 5.1. The four frames show the error in the field ($\delta B = B_{calculated} - B_{reconstructed}$) for different numbers of spectral components used. The curves where the field has been computed from only 4 and 22 spectral components show a significant deviation between the numerically integrated magnetic field and the reconstructed magnetic field. It is only when the number of spectral components exceeds 100 that the error δB is reduced to an appropriate level.

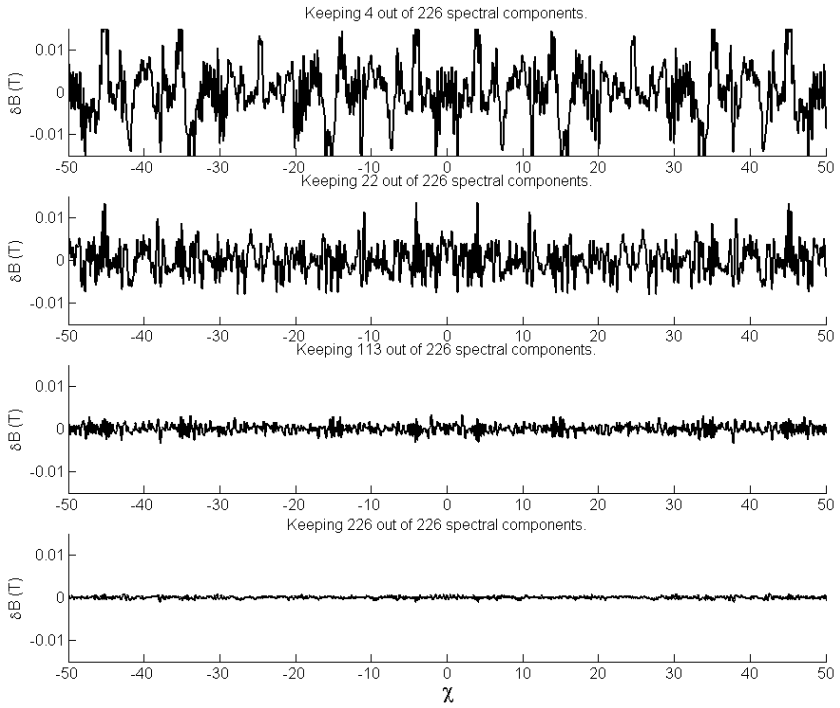

Figure 5.1: δB vs. χ curves for different numbers of spectral components.

The different choice of flux surface angles between the Hamada and Boozer coordinates lead to spectra that are slightly different. The difference between the Boozer and Hamada (n,m)=(4,1) mode is minor for the QHS case; at the edge, the difference is less than 1% of that mode's amplitude. This difference between the two spectra is more visible in the symmetry breaking. In particular, the three largest spectral components after the (4,1) component in the QHS Boozer spectrum on the LCFS are (n,m)=(12,3), (8,3), and (8,2), in order of decreasing mode amplitude. For the Hamada spectrum, the same criterion yields (8,2), (4,2), and (4,0). Further, the Boozer spectrum at the QHS LCFS has 8 components with m=0 in the first 30 largest components, while the Hamada spectrum has only 2. In particular, the (n,m)=(48,0) modular coil ripple component is very small in the Hamada spectrum.

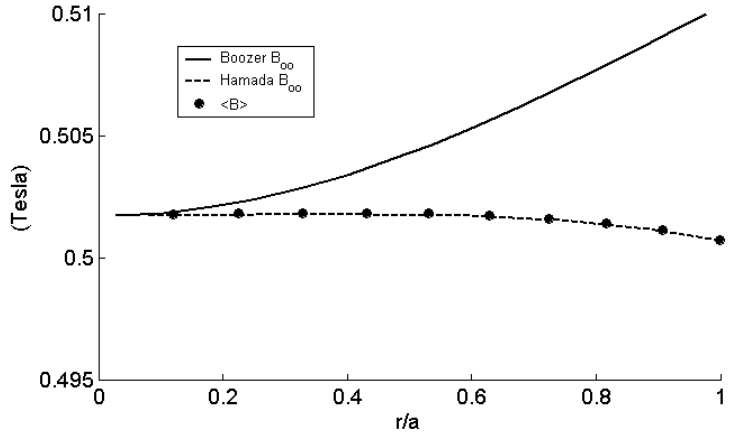

Figure 5.2: Radial dependence of the (n,m)=(0,0) spectral component in Boozer (solid) and Hamada (dashed) coordinates.

The (n,m)=(0,0) mode profile for the two types of spectra are shown in figure 5.2. They clearly have different magnitudes and radial dependencies. The Hamada B_{oo} is the actual average field on a flux surface. This can be observed if the Fourier expansion of B is inserted into the flux surface average

$$\langle B \rangle = \frac{\int_0^{2\pi}\int_0^{2\pi} \sqrt{g} B_o \sum_{n,m} b_{nm} \cos(n\zeta - m\alpha)\, d\alpha d\zeta}{\int_0^{2\pi}\int_0^{2\pi} \sqrt{g}\, d\alpha d\zeta}. \tag{5.28}$$

In Hamada coordinates, where the Jacobian is a flux surface quantity, this entire expression can be simplified to $\langle B \rangle = B_o b_{00}$. The same argument does not hold on Boozer coordinates, as the Jacobian is $\propto B^{-2}$ and cannot be factored out of the integration. The directly numerically calculated <B>, calculated as

$$\langle B \rangle = \lim_{N\to\infty} \frac{\int_0^N \frac{dl}{B} B}{\int_0^N \frac{dl}{B}}, \tag{5.29}$$

is also shown in figure 5.2, and it matches the Hamada (0,0) mode amplitude. Note that the two (0,0) components agree with each other near the axis, where the variation in B on the surface is vanishingly small.

5.3: Example Calculations of the Spectra

As discussed in great detail in Appendix 2 of this dissertation, there are many different configurations available to the HSX stellarator. The auxiliary coils can be used to introduce large symmetry breaking terms into the spectrum. The amplitude of these symmetry breaking terms can be changed, as can the dominant m and n numbers of the symmetry breaking. Alternatively, the auxiliary coils can be used to adjust the rotational transform over a large range. This section illustrates the changes in the magnetic field spectra in some of these different configurations.

To specify a configuration, it is sufficient to specify two items. The stencil array describes the direction of currents in the auxiliary coils compared to the main coils, and the amp-turn percentage defines the ratio of amp-turns in the auxiliary coil set to the main coils. There are four different stencil arrays that have been considered in this work, and they are contained in table 5.1. Note that the normal Mirror configuration of HSX is the Type 1 configuration in this description. Positive amp-turn percentages correspond to the Hill and Mirror configurations, while negative amp-turn percentages correspond to Well and antiMirror configurations.

Configuration	Coil 1	Coil 2	Coil 3	Coil 4	Coil 5	Coil 6
Mirror, Type 1	1	1	1	-1	-1	-1
Mirror, Type 2	1	-1	1	-1	1	-1
Mirror, Type 3	1	-1	-1	1	1	-1
Hill/Well	1	1	1	1	1	1

Table 5.1: Stencils for various configurations of HSX. The sign represents the direction of current in each auxiliary coil compared to the direction of current in the main coils.

In general, there are two means of breaking the quasi-symmetry in HSX. The symmetry can be broken on all flux surfaces at once by introducing large changes in the |B| around the machine without significantly changing the field line trajectory. An example of this is the (Type 1) Mirror configuration of HSX, where a large (n,m)=(4,0) component is introduced into the spectrum

without significantly changing the flux surface shape. The rotational transform profile for this configuration is shown on the left of figure 5.3, and the magnetic field spectrum is shown on the right. Note that (n,m)=(4,1) spectral component is augmented in this case by a large (4,0) spectral component, leading to a very large deviation from quasi-symmetry. The flux surface shape is quite similar for the QHS and 10% Type 1 Mirror configurations. The 12/11 resonance in the rotational transform profile does not cause a significant island chain, and is not studied in detail in this calculation. The transform is everywhere above 16/15 and beneath 8/7.

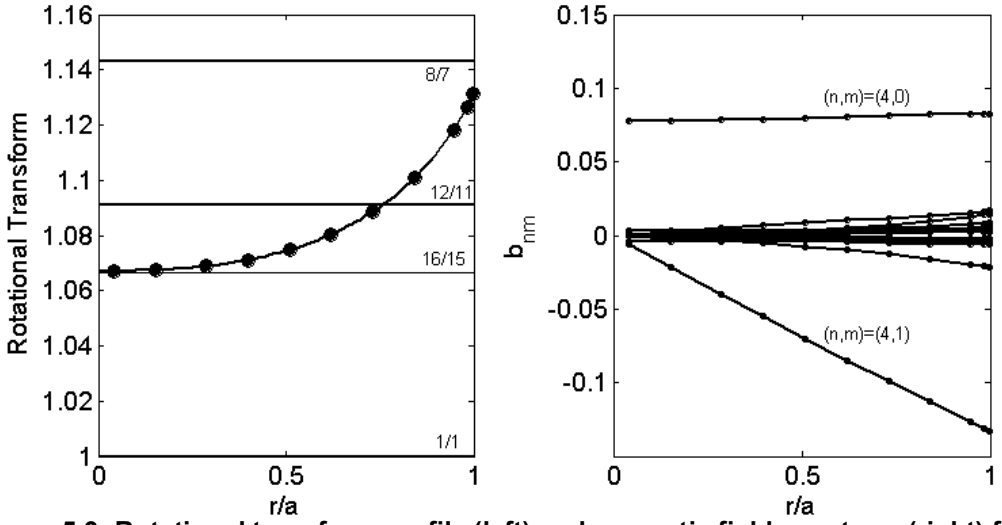

Figure 5.3: Rotational transform profile (left) and magnetic field spectrum (right) for the 10% Mirror case.

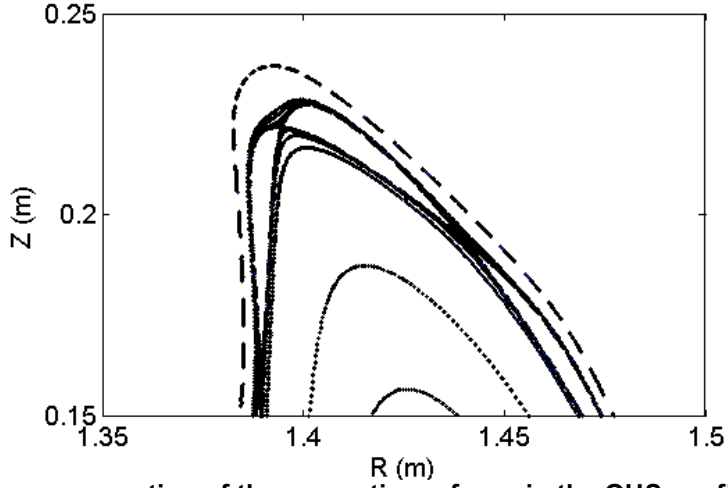

Figure 5.4: An upper portion of the magnetic surfaces in the QHS configuration in a vertical cut at the symmetry plane, illustrating the corrugation effect for surfaces very near the ι=12/11 island chain.

A second means of breaking the symmetry involves making small changes to the magnetic field which leave |B| mostly unchanged but cause large deviations of the field line trajectory. This occurs near a magnetic island. Flux surfaces just inside or outside of the magnetic island stay close to the island chain, leading to significant deviations from their shape if the island were not present. An example of this effect is shown for the QHS configuration of HSX in figure 5.4, for surfaces near the intrinsic ι=12/11 island chain. The outermost surface in this plot is the last closed flux surface.

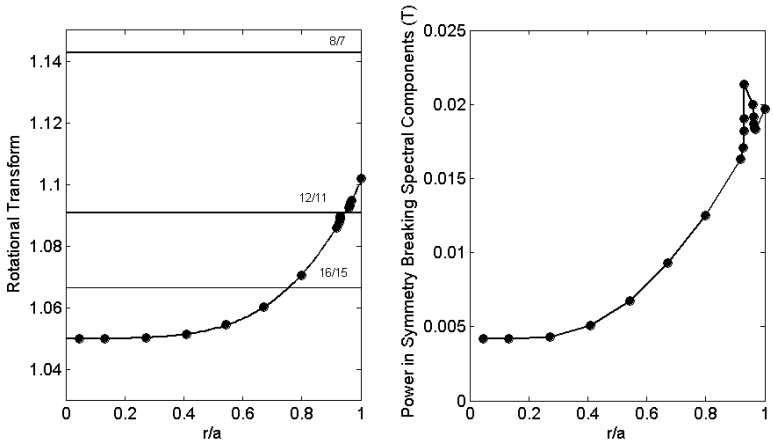

Figure 5.5: Rotational transform profile for the QHS configuration (left), and the power in symmetry breaking spectral components (right). The solid symbols correspond to the surfaces shown in figure 5.4.

The rotational transform for the QHS configuration is shown in the left frame of figure 5.5, along with horizontal lines representing the 8/7, 12/11, and 16/15 resonances. The 16/15 resonance does not cause a large island chain to develop, but the 12/11 resonance results in the islation visible in figure 5.4. As a figure of merit regarding symmetry breaking, the power in symmetry breaking spectral components can be defined as

$$\text{Power} = \left(\sum_{\substack{(n,m)\neq(0,0),(4,1) \\ n/4\neq m}} b_{n,m}^2 \right)^{1/2} . \qquad (5.30)$$

The right plot in figure 5.5 illustrates the power in symmetry breaking components as a function of radius for the QHS configuration. The power in such components increases significantly in the vicinity of the island chain.

The Hamada spectrum for the QHS configuration is shown in figure 5.6. The frame on the left illustrates the complete spectrum, where the quasi-symmetry is manifest in the dominance of the single term in the spectrum. The frame on the right has a much smaller y-axis range, allowing the symmetry breaking spectral components to be observed. Note that many of the spectral components are not impacted by the magnetic island, but that other terms become much larger near the island. The plots show the 10 spectral components with the largest absolute magnitude at r/a=0.96. Note the (-8,-10) and (16,12) components that are comparatively large in the vicinity of the island chain, but are otherwise small.

The mode numbers of these spectral components can be predicted by considering the interaction of the (n,m)=(12,11) islands with the (n,m)=(4,1) main helical component. The interaction will give rise to spectral components with mode numbers

$$(n,m) = (4,1) \pm (12,11) = (-8,-10),(16,12)$$

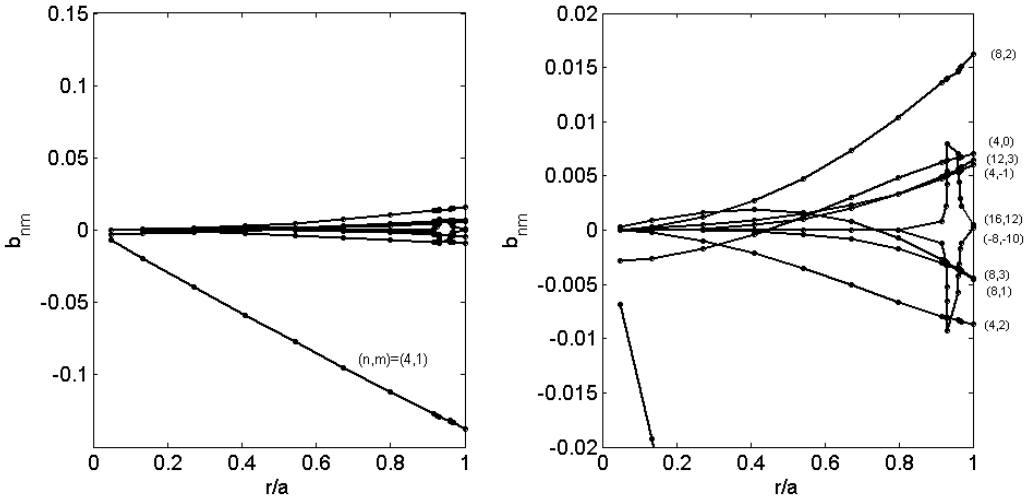

Figure 5.6: Complete Hamada spectra for the QHS case (left) and a restricted view illustrating the symmetry breaking terms near the magnetic island.

The most severe example of this symmetry breaking occurs in cases where the ι=4/4 island chain is present inside the LCFS. This occurs in the Hill mode for amp-turn percentages of ~6%. A plot of the flux surfaces for this case is shown in figure 5.7, where the large vacant spaces in the plot correspond to the locations of the four large magnetic islands. There is severe distortion of the magnetic surfaces near the island chain. These distortions give rise to large symmetry breaking spectral components, especially in the form of (n,m)=(8,5), (12,6), and (12,9) spectral components just outside of the island chain, as illustrated in figure 5.8. Note that due to the changes in magnetic surface shape across the island, the spectral component amplitudes are not continuous functions of normalized toroidal flux.

As with the QHS case, these spectral components can be considered as the interaction of the (n,m)=(4,1) helical component with the both the (4,4) perturbation and higher harmonics of the perturbation.

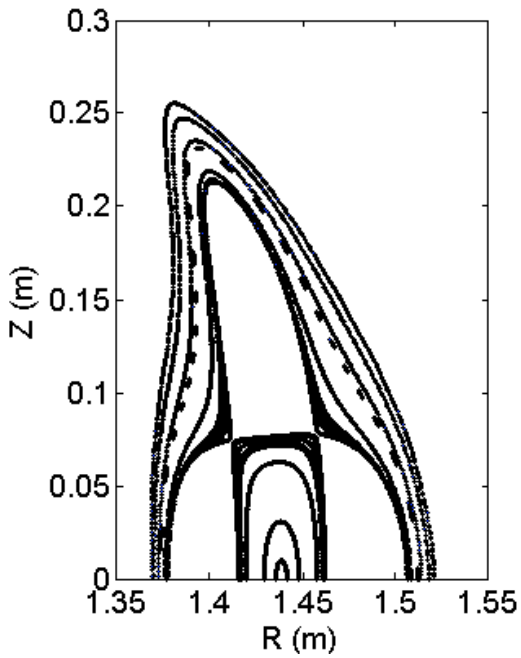

Figure 5.7: A portion of the magnetic surfaces in the 6% hill configuration, illustrating the ι=4/4 island chain and the severe distortion of the island near that surface.

Further discussion of these magnetic configurations will be presented in later sections. The impact of symmetry breaking perturbations on viscous damping will be discussed in

Appendix 5. Those discussions will concentrate on both viscous damping due to Mirror like perturbations and magnetic island induced viscous damping. Detailed information regarding the different magnetic configurations of HSX is provided in Appendix 2 of this document.

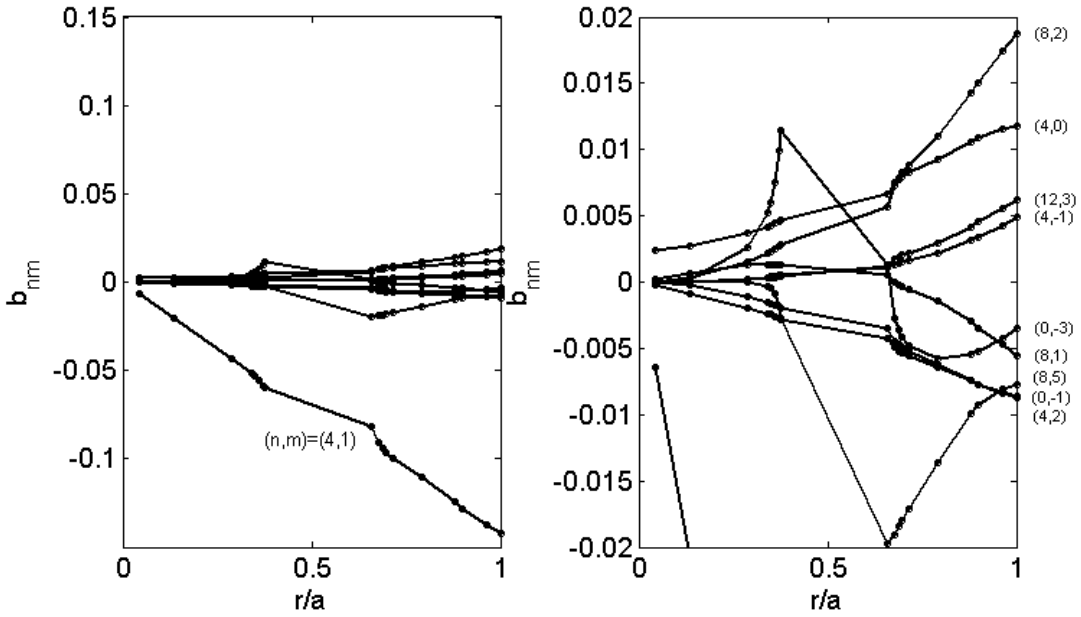

Figure 5.8: Complete Hamada spectra for the 6% Hill case (left) and a restricted view (right) illustrating the symmetry breaking terms near the magnetic island.

5.4: The Technique for Calculating the Hamada Basis Vectors

This section will provide details on the calculation of the Hamada basis vectors for arbitrary toroidal geometry. In 5.4.1, the general structure of the method is laid out in detail. It will be shown that there are nine initial conditions on the basis vectors which must be known before the calculation begins. Section 5.4.2 illustrates the reduction from nine unknowns to a single unknown. This single unknown can be calculated based on two different methods of calculating the Pfirsch-Schlueter current. These two methods are discussed in 5.4.3 and 5.4.4, and their

synthesis to resolve the last initial condition is discussed in 5.4.5. A calculation for the QHS configuration of HSX is presented in Section 5.4.6 as an example.

5.4.1 Method of Numerically Calculating the Contravariant Basis Vectors.

The general procedure for calculating the contravariant Hamada basis vectors is based on the work by Nemov.[4] The problem is to find a general method of calculating $\nabla\rho$, $\nabla\alpha$, and $\nabla\zeta$ based on calculation of the vector magnetic field from a Biot-Savart code. These contravariant basis vectors are related to the Jacobian and rotational transform as

$$\mathbf{B}\cdot\nabla\rho = 0\,, \tag{5.31}$$

$$\mathbf{B}\cdot\nabla\zeta = \frac{1}{2\pi\sqrt{g}}\,, \tag{5.32}$$

$$\mathbf{B}\cdot\nabla\alpha = \frac{\iota}{2\pi\sqrt{g}}\,. \tag{5.33}$$

Each of these equations is a magnetic differential equation of the form

$$B^f = \mathbf{B}\cdot\nabla f = S_f(\rho), \tag{5.34}$$

where f={ρ,α,ζ} and the source terms are

$$S_f = \left\{0, \frac{1}{2\pi\sqrt{g}}, \frac{\iota}{2\pi\sqrt{g}}\right\}. \tag{5.35}$$

To solve this equation, we proceed by breaking ∇f into its components in the laboratory cylindrical coordinate system

$$\nabla f = P_f\hat{\mathbf{R}} + \frac{Q_f}{R}\hat{\boldsymbol{\Phi}} + G_f\hat{\mathbf{Z}}\,, \tag{5.36}$$

with $P_f=\partial f/\partial R$, $Q_f=\partial f/\partial\Phi$, and $G_f=\partial f/\partial Z$ and the hats denoting unit vectors. This enables the governing magnetic differential equations to be written as

$$\mathbf{B}\cdot\nabla f = P_f B_R + \frac{Q_f}{R}B_\Phi + G_f B_Z = S_f(\rho). \tag{5.37}$$

When this equation is differentiated with respect to R, the result is

$$\frac{\partial P_f}{\partial R}B_R + \frac{\partial Q_f}{\partial R}\frac{B_\Phi}{R} + \frac{\partial G_f}{\partial R}B_Z = \frac{\partial S_f}{\partial R} - \left(P_f\frac{\partial B_R}{\partial R} + Q_f\frac{\partial}{\partial R}\left(\frac{B_\Phi}{R}\right) + G_f\frac{\partial B_Z}{\partial R}\right). \tag{5.38}$$

This equation can be simplified using the equality of mixed partial derivatives on the left hand side. After differentiation of (5.38) with respect to Φ and Z, the following system of equations is derived

$$\mathbf{B}\cdot\nabla P_f = \frac{\partial S_f}{\partial R} - \left(P_f\frac{\partial B_R}{\partial R} + Q_f\frac{\partial}{\partial R}\left(\frac{B_\Phi}{R}\right) + G_f\frac{\partial B_Z}{\partial R}\right), \tag{5.39a}$$

$$\mathbf{B}\cdot\nabla Q_f = \frac{\partial S_f}{\partial \Phi} - \left(P_f\frac{\partial B_R}{\partial \Phi} + Q_f\frac{\partial}{\partial \Phi}\left(\frac{B_\Phi}{R}\right) + G_f\frac{\partial B_Z}{\partial \Phi}\right), \tag{5.39b}$$

$$\mathbf{B}\cdot\nabla G_f = \frac{\partial S_f}{\partial Z} - \left(P_f\frac{\partial B_R}{\partial Z} + Q_f\frac{\partial}{\partial Z}\left(\frac{B_\Phi}{R}\right) + G_f\frac{\partial B_Z}{\partial Z}\right). \tag{5.39c}$$

Note that there are a total of nine equations in the full problem, with three for each of f={ρ,ζ,α}. The solution of these nine equations yields the lab frame components of the contravariant basis vectors.

Each of these nine equations can be solved along a field line. Consider a general magnetic differential equation of the form

$$\mathbf{B}\cdot\nabla\xi = F. \tag{5.40}$$

This can be written as

$$B_R\frac{\partial\xi}{\partial R} + \frac{B_\phi}{R}\frac{\partial\xi}{\partial\phi} + B_Z\frac{\partial\xi}{\partial Z} = F. \tag{5.41}$$

Taking the total derivative $d\xi/d\phi$ and using the equations of a field line leads to the relationship

$$\frac{\partial \xi}{\partial \phi} = \frac{d\xi}{d\phi} - \frac{\partial \xi}{\partial R} R \frac{B_R}{B_\phi} - \frac{\partial \xi}{\partial Z} R \frac{B_Z}{B_\phi}. \tag{5.42}$$

When this expression is inserted in (5.40), the simplified result is that ξ can be solved along a field line by solving the coupled differential equations.

$$\frac{dR}{d\phi} = R \frac{B_R}{B_\phi}, \tag{5.43a}$$

$$\frac{dZ}{d\phi} = R \frac{B_Z}{B_\phi}, \tag{5.43b}$$

$$\frac{d\xi}{d\phi} = \frac{R}{B_\phi} F. \tag{5.43c}$$

It is assumed that the value of ξ is known at the starting point of the integration. Hence, it is necessary to know the values of the components of $\nabla\psi$, $\nabla\alpha$, and $\nabla\zeta$ at the starting point of the integration. This is the initial condition problem which will be studied in the next section.

The solution of equations (5.31)-(5.33) requires the calculation of terms like dS/dZ, dS/dΦ, and dS/dR, where S is defined in (5.35). These can be calculated as, for example,

$$\frac{\partial S_\alpha}{\partial R} = \frac{1}{2\pi\sqrt{g}} \frac{\partial \psi}{\partial R} \left(\frac{\partial \iota}{\partial \psi} - \frac{\iota}{\sqrt{g}} \frac{\partial \sqrt{g}}{\partial \psi} \right). \tag{5.44}$$

The term $\partial\psi/\partial R = P_\psi$ is calculated as the integration progresses. Hence, it is only necessary to know the derivatives of the rotational transform and Jacobian with respect to ψ when computing the derivatives of the source terms.

For the neoclassical modeling which motivates this calculation, it is necessary to evaluate the following flux surface averages

$$\begin{array}{ccc} \langle \mathbf{e}_\alpha \cdot \mathbf{e}_\alpha \rangle & \langle \mathbf{e}_\zeta \cdot \mathbf{e}_\alpha \rangle & \langle \mathbf{e}_\zeta \cdot \mathbf{e}_\zeta \rangle \\ \langle f_n(\alpha,\zeta) \mathbf{e}_\alpha \cdot \mathbf{e}_\alpha \rangle & \langle f_n(\alpha,\zeta) \mathbf{e}_\zeta \cdot \mathbf{e}_\alpha \rangle & \langle f_n(\alpha,\zeta) \mathbf{e}_\zeta \cdot \mathbf{e}_\zeta \rangle \\ \langle |\nabla\psi| \rangle & \langle \nabla\psi \cdot \nabla\psi \rangle & \\ \langle B_\alpha \rangle & \langle B_\zeta \rangle & \end{array}$$

Here, $f_n(\alpha,\zeta)$ is a function representing the distribution of neutral hydrogen around HSX. Each of the quantities within the brackets can be calculated along a field line using the technique discussed above. These flux surface averages can be easily calculated by noting that

$$\left\langle f \right\rangle = \lim_{\#\text{transits}\to\infty} \frac{\int f \frac{dl}{B}}{\int \frac{dl}{B}}. \tag{5.45}$$

If the definitions $g=\int f dl/B$ and $g_n=\int dl/B$ are used, then it can be shown that $B\cdot\nabla g=f$ and $B\cdot\nabla g_n=1$. These two equations can be solved along a field line as the basis vectors are being calculated using the method described near equation (5.40), and the flux surface average calculated as $\langle f\rangle=g/g_n$. Note that this process requires solving ten differential equations for the averaged quantities plus the normalization g_n.

This numerical technique also makes possible an accurate calculation of the area of a flux surface. The flux surface average of a quantity Φ is given by:

$$\left\langle \Phi \right\rangle = \frac{d\psi}{dV} \iint_{S(\psi)} \Phi \frac{dS}{|\nabla\psi|}. \tag{5.46}$$

Inserting $\Phi=|\nabla\psi|$ into this expression yields

$$\left\langle |\nabla\psi| \right\rangle = \frac{d\psi}{dV} \iint_{S(\psi)} dS. \tag{5.47}$$

Noting that the area of the surface is simply $A=\iint dS$ and using (5.9) yields an expression for the flux surface area as

$$A = \left\langle |\vec{\nabla}\psi| \right\rangle 4\pi^2 \sqrt{g}. \tag{5.48}$$

In summary, there are 22 simultaneous differential equations to be solved. There are two equations for the field line trajectory and nine equations for the components of the basis vectors. There are ten equations for the ten flux surface averages, as well as one equation to normalize the flux surface averages.

A few practical notes about the calculation are in order. It is critically important to have accurate values of the derivatives of the rotational transform and Jacobian with respect to toroidal flux. It is generally acceptable to calculate the flux, Jacobian and transform on the surface where the basis vectors will be calculated, as well as two surfaces on either side (.25mm separation in the case of the calculations presented here). The derivatives noted above can then be calculated based on these closely spaced surfaces. It is generally not acceptable to calculate the rotational transform from puncture plot methods; the rotational transform calculation from the Hamada or Boozer spectrum calculation works much better. During the actual integration, the values of the basis vectors and other quantities are recorded at $\Phi=n\pi/2$, with n an integer, corresponding to the four symmetry planes of the machine. Calculation of the basis vectors at other places in the machine (the location of a probe for instance) requires a second integration of these equations. The integration in done with the ODE113 integration routine, with an absolute tolerance of 10^{-11} and a relative tolerance of 10^{-9}. It is important to use closed coils when calculating the magnetic field. The magnetic field calculated from open coil models does not satisfy $\nabla\cdot\mathbf{B}=0$, and will lead to unphysical results in the basis vector calculation.

5.4.2: Reduction from Nine to One Unknown Initial Conditions

To numerically integrate the nine equations for the components of the Hamada basis vectors (5.39), it is necessary to know the values of all nine components at some location in the machine. The integration then proceeds forward from this location. The method for calculating these initial conditions is described in this section. Simple geometric arguments will be made to reduce the number of unknowns from nine to four. Expressions for the Jacobian and the contravariant field components will yield three expressions relating these final four unknowns. A final relationship will be derived in the following two subsections based upon two different expressions for the Pfirsch-Schlueter current in 3D toroidal geometry.

The calculation always starts at the outboard midplane of HSX at the elliptical symmetry plane of a box port. At this location, $\nabla\psi$ points outward along the **R** axis. With this knowledge, it is

possible to immediately set Q_ψ=G_ψ=0 at this location. Further, the magnetic field has no **R** component at this location, i.e. $\mathbf{B}=B_\Phi\mathbf{\Phi}+B_Z\mathbf{Z}$. If the magnetic field along the R axis is written as

$$\mathbf{B}=\hat{\mathbf{R}}\left(B_\alpha P_\alpha+B_\zeta P_\zeta+B_\psi P_\psi\right)+\frac{\hat{\mathbf{O}}\left(B_\alpha Q_\alpha+B_\zeta Q_\zeta\right)}{R}+\hat{\mathbf{Z}}\left(B_\alpha G_\alpha+B_\zeta G_\zeta\right), \tag{5.49}$$

then the condition that B_R=0 can be satisfied by setting P_α=P_ζ=B_ψ=0. P_ψ=$\partial\psi/\partial$R can be calculated from the toroidal flux enclosed in a Poincarre plot. With these observations, the nine unknowns are reduced to four: Q_ζ, G_ζ, Q_α, and G_α.

A series of relationships can be found between these quantities. The relationships (5.32) and (5.33) can be used to derive the relationships

$$\frac{B_\Phi}{R}Q_\zeta+B_Z G_\zeta=B^\zeta, \tag{5.50}$$

$$\frac{B_\Phi}{R}Q_\alpha+B_Z G_\alpha=B^\alpha. \tag{5.51}$$

Finally, the definition of the Jacobian can be used to show that

$$-G_\zeta Q_\alpha+Q_\zeta G_\alpha=\frac{R}{\sqrt{g}P_\psi}. \tag{5.52}$$

These three expressions relate the four unknowns, leaving the problem with the need for one more expression relating the quantities. This final expression will be derived by equating a numerical calculation of the Pfirsch-Schlueter current to an analytic one.

5.4.3: The Numerical Calculation of the Pfirsch-Schlueter Currents.

The means of numerically calculating the Pfirsch-Schlueter current is due to Nemov.[5] This method begins with the MHD equilibrium expression

$$\nabla p=\mathbf{J}\times\mathbf{B}. \tag{5.53}$$

By writing ∇p=(∂p/$\partial\psi$)$\nabla\Psi$ and taking B×(5.53), it is possible to solve for the perpendicular currents as

$$\mathbf{J}_{\perp} = \frac{\partial p}{\partial \psi}\frac{\mathbf{B}\times\nabla\psi}{B^2}. \tag{5.54}$$

The incompressibility of current flow can be written as $\nabla\cdot\mathbf{J}=0$. By writing $\mathbf{J}=\mathbf{J}_{\perp}+J_{||}\mathbf{B}/B$, a relationship between the perpendicular and parallel currents can be found as

$$\nabla\cdot\mathbf{J}_{\perp} = -\mathbf{B}\cdot\nabla\left(\frac{J_{||}}{B}\right). \tag{5.55}$$

The expression for $\nabla\cdot\mathbf{J}_{\perp}$ can be written from (5.54) as

$$\nabla\cdot\mathbf{J}_{\perp} = \frac{\partial p}{\partial \psi}\frac{1}{B^2}\nabla\cdot(\mathbf{B}\times\nabla\psi)+\mathbf{B}\times\nabla\psi\cdot\nabla\left(\frac{\partial p}{\partial \psi}\frac{1}{B^2}\right). \tag{5.56}$$

The first term on the RHS can be eliminated by noting that

$$\nabla\cdot(\mathbf{B}\times\nabla\psi)=\mathbf{B}\cdot(\nabla\times\nabla\psi)-\nabla\psi\cdot\nabla\times\mathbf{B}=0. \tag{5.57}$$

The second term on the RHS can be simplified by noting

$$\mathbf{B}\times\nabla\psi\cdot\nabla\left(\frac{\partial p}{\partial \psi}\frac{1}{B^2}\right) = -\frac{2}{B^3}\frac{\partial p}{\partial \psi}\nabla B\cdot(\mathbf{B}\times\nabla\psi). \tag{5.58}$$

This allows (5.56) to be written as

$$\mathbf{B}\cdot\nabla\left(\frac{J_{||}}{B}\right) = \frac{2}{B^3}\frac{\partial p}{\partial \psi}\nabla B\cdot(\mathbf{B}\times\nabla\psi). \tag{5.59}$$

Finally, by defining $J_{||}=hB(\partial p/\partial\psi)$, it is possible to write

$$\mathbf{B}\cdot\nabla h = \frac{2}{B^3}\nabla B\cdot(\mathbf{B}\times\nabla\psi). \tag{5.60}$$

This equation can be used to evolve h along a field line using the techniques described in Section 5.4.1. The value of h at some initial location must be known. To find this initial condition, consider that the parallel current must be driven by some potential on a flux surface:

$$\mathbf{J}_{||} = -\sigma_{||}\nabla\Phi. \tag{5.61}$$

For this potential to be single valued, it must satisfy $\langle \mathbf{B}\cdot\nabla\Phi\rangle=0$. Assuming that the integration of (5.60) is done in toroidal angle, we can write $h=h_o+h_s(\Phi)$ where h_o is the initial condition on h which we need to calculate. Inserting this expression into $\langle B\cdot\nabla\Phi\rangle=0$ yields

$$\left\langle \mathbf{B}\cdot\vec{\nabla}\Phi\right\rangle = -\frac{\partial p}{\partial\psi}\frac{1}{\sigma_{||}}\left\langle \left(h_o + h_s(\Phi)\right)B^2\right\rangle . \tag{5.62}$$

Computing the flux surface average as

$$\left\langle \left(h_o + h_s(\Phi)\right)B^2\right\rangle = \frac{\int\frac{dl}{B}\left(h_o + h_s(\Phi)\right)B^2}{\int\frac{dl}{B}}, \tag{5.63}$$

it can be seen that the condition $\langle \mathbf{B}\cdot\nabla\Phi\rangle=0$ reduces to

$$\int\frac{dl}{B}\left(h_o + h_s(\Phi)\right)B^2 = 0 . \tag{5.64}$$

Hence, it is possible to calculate

$$h_o = -\frac{\Phi_1}{\Phi_2}, \tag{5.65}$$

where Φ_1 and Φ_2 are calculated by solving the magnetic differential equation

$$\mathbf{B}\cdot\nabla\Phi_1 = h_s B^2, \tag{5.66a}$$

$$\mathbf{B}\cdot\nabla\Phi_2 = B^2, \tag{5.66b}$$

with $h_s(\Phi)$ calculated using (5.60). This h_o will be the fundamental quantity of interest in these calculations

In summary, the Pfirsch-Schlueter current is calculated by integrating the following eight equations:

$$\frac{dR}{d\Phi} = \frac{RB_R}{B_\Phi}, \tag{5.67a}$$

$$\frac{dZ}{d\Phi} = \frac{RB_Z}{B_\Phi}, \tag{5.67b}$$

$$\frac{dP_\psi}{d\Phi} = -\frac{R}{B_\Phi}\left(P_\psi \frac{\partial B_R}{\partial R} + Q_\psi \frac{\partial}{\partial R}\left(\frac{B_\phi}{R}\right) + G_\psi \frac{\partial B_Z}{\partial R}\right), \tag{5.67c}$$

$$\frac{dQ_\psi}{d\Phi} = -\frac{R}{B_\Phi}\left(P_\psi \frac{\partial B_R}{\partial \Phi} + Q_\psi \frac{\partial}{\partial \Phi}\left(\frac{B_\phi}{R}\right) + G_\psi \frac{\partial B_Z}{\partial \Phi}\right), \tag{5.67d}$$

$$\frac{dG_\psi}{d\Phi} = -\frac{R}{B_\Phi}\left(P_\psi \frac{\partial B_R}{\partial Z} + Q_\psi \frac{\partial}{\partial Z}\left(\frac{B_\phi}{R}\right) + G_\psi \frac{\partial B_Z}{\partial Z}\right), \tag{5.67e}$$

$$\frac{dh_s}{d\Phi} = \frac{R}{B_\Phi}\frac{2}{B^3}\nabla B \cdot (\mathbf{B} \times \nabla\psi), \tag{5.67f}$$

$$\frac{d\Phi_1}{d\Phi} = \frac{R}{B_\Phi} h_s B^2, \tag{5.67g}$$

$$\frac{d\Phi_2}{d\Phi} = \frac{R}{B_\Phi} B^2. \tag{5.67h}$$

The calculation is always started from the outboard midplane where the initial conditions on the components of $\nabla\psi$ are known. The integration is usually computed for 100 toroidal transits, with an absolute integration tolerance of 10^{-11} and a relative integration tolerance of 10^{-9}, using the Matlab ODE113 integration routine.

An example of the convergence of Φ_1/Φ_2 is shown in figure 5.9, for a surface near the edge for the QHS case. Many toroidal transits are necessary to achieve convergence of this ratio. The ratio converges more quickly for surfaces nearer the magnetic axis than for those near the edge.

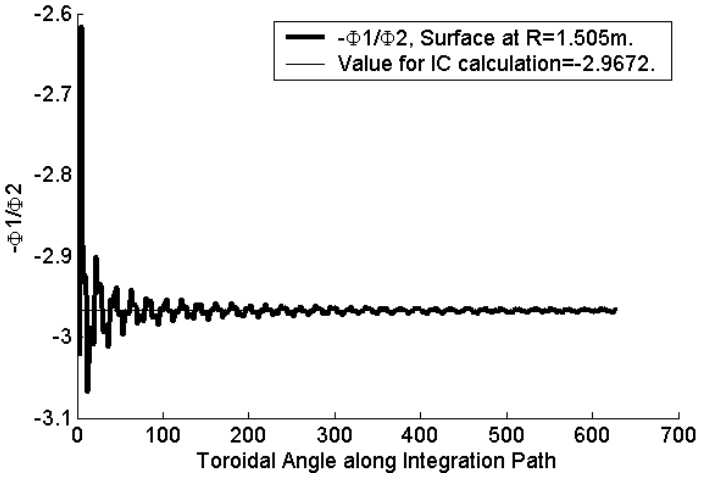

Figure 5.9: Convergence of the ratio Φ_1/Φ_2 as a function of length along the integration path.

The normalized Pfirsch-Schlueter current hB is shown in figure 5.10 as a function of laboratory poloidal angle. In this plot and those to follow, the lab frame poloidal angle is defined as θ_{lab}=atan((Z-Z_{axis})/(R-R_{axis})). The plot is for the QHS configuration for a field line launched at R=1.505, corresponding to r/a~0.85. The current does not have the simple cos(θ) dependence as expected from a tokamak expression.

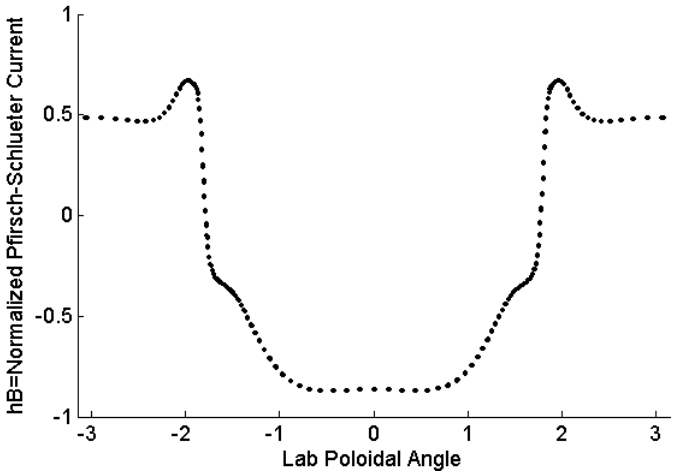

Figure 5.10: hB, the normalized Pfirsch-Schlueter current.

5.4.4: The Analytic Calculation of the Pfirsch-Schlueter Currents.

Analytic expressions for the Pfirsch-Schlueter current in non-axisymmetric toroidal geometry appear in Shaing and Callen[6] and in Coronado and Wobig.[7] The development here will closely follow the later development. Note that the cyclic order of the Hamada Coordinates is different here than in the original work by Coronado and Wobig, and that their flux surface angles vary as $0<\alpha,\zeta<1$, not $0<\alpha,\zeta<2\pi$ as in this calculation.

The derivation starts with the perpendicular currents from the lowest order MHD equilibrium:

$$\mathbf{J}_{\perp} = \frac{\partial p}{\partial \psi}\frac{\mathbf{B}\times\nabla\psi}{B^2}. \tag{5.68}$$

The vector parallel currents are written as $\mathbf{J}_{\|}=f\mathbf{B}$, allowing $\nabla\cdot\mathbf{J}=0$ to be written as

$$\mathbf{B}\cdot\nabla f = -\frac{\partial p}{\partial \psi}\nabla\cdot\left(\frac{\mathbf{B}\times\nabla\psi}{B^2}\right). \tag{5.69}$$

To solve for f, the equation can be simplified as follows. Using the relationships

$$\nabla\alpha\times\nabla\psi = \frac{\mathbf{e}_{\zeta}}{\sqrt{g}}, \tag{5.70}$$

$$\nabla\zeta\times\nabla\psi = -\frac{\mathbf{e}_{\alpha}}{\sqrt{g}}, \tag{5.71}$$

it is possible to show that

$$\frac{\mathbf{B}\times\nabla\psi}{B^2} = \frac{B_{\alpha}\mathbf{e}_{\zeta} - B_{\zeta}\mathbf{e}_{\alpha}}{B^2\sqrt{g}}. \tag{5.72}$$

This expression, along with $\nabla\cdot(\mathbf{e}_{\alpha}/\sqrt{g})= \nabla\cdot(\mathbf{e}_{\zeta}/\sqrt{g})=0$, allows the divergence term in (5.69) to be expressed as

$$\nabla\cdot\frac{\nabla\psi\times\mathbf{B}}{B^2} = \frac{1}{\sqrt{g}}\left(\mathbf{e}_{\alpha}\cdot\nabla\frac{B_{\zeta}}{B^2} - \mathbf{e}_{\zeta}\cdot\nabla\frac{B_{\alpha}}{B^2}\right). \tag{5.73}$$

Next, consider a term of the form $\mathbf{B}\cdot\nabla(B_{\alpha}/B^2B^{\zeta}\sqrt{g})$. This term can be written as

$$\mathbf{B}\cdot\nabla\frac{B_\alpha}{B^2B^\zeta\sqrt{g}}=\left(B^\zeta\mathbf{e}_\zeta+B^\alpha\mathbf{e}_\alpha\right)\cdot\nabla\left(\frac{B^2-B^\zeta B_\zeta}{B^2B^\zeta B^\alpha\sqrt{g}}\right). \tag{5.74}$$

Further simplification of this expression yields

$$\mathbf{B}\cdot\nabla\frac{B_\alpha}{B^2B^\zeta\sqrt{g}}=B^\zeta\mathbf{e}_\zeta\cdot\nabla\frac{B_\zeta}{B^2B^\zeta\sqrt{g}}-B^\alpha\mathbf{e}_\alpha\cdot\nabla\frac{B_\alpha}{B^2B^\alpha\sqrt{g}}. \tag{5.75}$$

This can be simplified by the fact that the contravariant field components and the Jacobian are flux surface quantities in Hamada Coordinates:

$$\mathbf{B}\cdot\nabla\frac{B_\alpha}{B^2B^\zeta\sqrt{g}}=\frac{\mathbf{e}_\zeta}{\sqrt{g}}\cdot\nabla\frac{B_\zeta}{B^2}-\frac{\mathbf{e}_\alpha}{\sqrt{g}}\cdot\nabla\frac{B_\alpha}{B^2}. \tag{5.76}$$

In comparing this expression to (63), it can be seen that

$$\nabla\cdot\frac{\nabla\psi\times\mathbf{B}}{B^2}=-\mathbf{B}\cdot\nabla\frac{B_\alpha}{B^2B^\zeta\sqrt{g}}. \tag{5.77}$$

Using similar algebra, it can be shown that

$$\nabla\cdot\frac{\nabla\psi\times\mathbf{B}}{B^2}=\mathbf{B}\cdot\nabla\frac{B_\zeta}{B^2B^\alpha\sqrt{g}}. \tag{5.78}$$

It can now be seen that the term $\mathbf{B}\cdot\nabla f$ can be written as the superposition of these two terms, with weighting factors a_1 and a_2 chosen such that $a_1+a_2\neq0$.

$$\mathbf{B}\cdot\nabla f=\frac{\partial p}{\partial\psi}\left(\frac{a_2}{a_1+a_2}\mathbf{B}\cdot\nabla\frac{B_\zeta}{B^2B^\alpha\sqrt{g}}-\frac{a_1}{a_1+a_2}\mathbf{B}\cdot\nabla\frac{B_\alpha}{B^2B^\zeta\sqrt{g}}\right). \tag{5.79}$$

The solution for $J_{||}$ can be seen from inspections as

$$\mathbf{J}_{||}=\frac{\mathbf{B}}{B^2\sqrt{g}}\frac{\partial p}{\partial\psi}\left(\frac{a_2}{a_1+a_2}\frac{B_\zeta}{B^\alpha}-\frac{a_1}{a_1+a_2}\frac{B_\alpha}{B^\zeta}\right)+\Lambda(\psi)\mathbf{B}. \tag{5.80}$$

In this equation, Λ is an integration constant related to Ohmic and bootstrap currents. Using the now known expressions for $J_{||}$ and $J_\perp$, the contravariant components of the current can be

calculated. Considering first the poloidal direction, the separate contravariant poloidal components of the parallel and perpendicular currents are given by

$$\mathbf{J}_{\|}\cdot\nabla\alpha=\frac{B^{\alpha}}{B^{2}\sqrt{g}}\frac{\partial p}{\partial\psi}\left(\frac{a_{2}}{a_{1}+a_{2}}\frac{B_{\zeta}}{B^{\alpha}}-\frac{a_{1}}{a_{1}+a_{2}}\frac{B_{\alpha}}{B^{\zeta}}\right)+\Lambda(\psi)B^{\alpha}, \tag{5.81}$$

$$\mathbf{J}_{\perp}\cdot\nabla\alpha=-\frac{B_{\zeta}}{B^{2}\sqrt{g}}\frac{\partial p}{\partial\psi}. \tag{5.82}$$

Adding these yields the total contravariant poloidal current

$$\mathbf{J}\cdot\nabla\alpha=-\frac{1}{B^{\zeta}\sqrt{g}}\frac{\partial p}{\partial\psi}\frac{a_{1}}{a_{1}+a_{2}}+\Lambda(\psi)B^{\alpha}. \tag{5.83}$$

The contravariant toroidal components of the parallel and perpendicular currents are

$$\mathbf{J}_{\perp}\cdot\nabla\zeta=\frac{B_{\alpha}}{B^{2}\sqrt{g}}\frac{\partial p}{\partial\psi}, \tag{5.84}$$

$$\mathbf{J}_{\|}\cdot\nabla\zeta=\frac{B^{\zeta}}{B^{2}\sqrt{g}}\frac{\partial p}{\partial\psi}\left(\frac{a_{2}}{a_{1}+a_{2}}\frac{B_{\zeta}}{B^{\alpha}}-\frac{a_{1}}{a_{1}+a_{2}}\frac{B_{\alpha}}{B^{\zeta}}\right)+\Lambda(\psi)B^{\zeta}. \tag{5.85}$$

Adding these yields the total contravariant toroidal current

$$\mathbf{J}\cdot\nabla\zeta=\frac{1}{B^{a}\sqrt{g}}\frac{\partial p}{\partial\psi}\frac{a_{2}}{a_{1}+a_{2}}+\Lambda(\psi)B^{\zeta}. \tag{5.86}$$

Note that both J^{α} and J^{ζ} are flux surface quantities; the current lines are straight lines in α,ζ coordinates, as predicted in Section 5.1. This is a defining feature of this coordinate system.

The net toroidal current is given by

$$I_{T}(\psi)=\int_{0}^{\psi}\int_{0}^{2\pi}\mathbf{J}\cdot d\mathbf{S}_{\zeta}, \tag{5.87}$$

where $d\mathbf{S}_{\zeta}=(\mathbf{e}_{\alpha}\times\mathbf{e}_{\psi})d\alpha d\psi$ is the surface element in the ζ direction. Using this expression for the differential surface area, differentiating with respect to ψ, and doing the integral over α yields

$$\frac{\partial I_T(\psi)}{\partial \psi} = 2\pi\sqrt{g}\left(\frac{a_2}{a_1 + a_2}\frac{1}{B^{\alpha}\sqrt{g}}\frac{\partial p}{\partial \psi} + \Lambda(\psi)B^{\zeta}\right). \tag{5.88}$$

This equation can be solved for $\Lambda(\psi)$ yielding

$$\Lambda(\psi) = \frac{1}{2\pi\sqrt{g}B^{\zeta}}\left(\frac{\partial I_T(\psi)}{\partial \psi} - \frac{a_2}{a_1 + a_2}\frac{\partial p}{\partial \psi}\frac{2\pi}{B^{\alpha}}\right). \tag{5.89}$$

When this is inserted into the expression for the toroidal and poloidal currents, they yield

$$\mathbf{J}\cdot\nabla\zeta = \frac{1}{2\pi\sqrt{g}}\frac{\partial I_T}{\partial \psi}, \tag{5.90}$$

$$\mathbf{J}\cdot\nabla\alpha = -\frac{1}{B^{\zeta}\sqrt{g}}\frac{\partial p}{\partial \psi} + \frac{B^{\alpha}}{B^{\zeta}}\frac{1}{2\pi\sqrt{g}}\frac{\partial I_T}{\partial \psi}. \tag{5.91}$$

These expressions show that the diamagnetic current and return currents (Pfirsch-Schlueter currents) are entirely contained in the poloidal component of the net current. With these expressions, the parallel current density can be written as

$$\mathbf{J}_{\|} = -\frac{B_{\alpha}}{B^2 B^{\zeta}\sqrt{g}}\frac{\partial p}{\partial \psi}\mathbf{B} + \frac{1}{2\pi B^{\zeta}\sqrt{g}}\frac{\partial I_T}{\partial \psi}\mathbf{B}. \tag{5.92}$$

In a net toroidal current free device, this expression reduces to

$$\mathbf{J}_{\|} = -\frac{B_{\alpha}}{B^2 B^{\zeta}\sqrt{g}}\frac{\partial p}{\partial \psi}\mathbf{B}. \tag{5.93}$$

5.4.5: Synthesizing the Two Calculations.

Having completed the two calculations of the Pfirsch-Schlueter current, it is necessary to synthesize them into a form where the final initial condition for the Hamada basis vector calculation can be derived. The two calculations of the Pfirsch-Schlueter current yielded two different expressions:

$$\mathbf{J}_{||} = -\frac{B_\alpha}{B^2 B^\zeta \sqrt{g}} \frac{\partial p}{\partial \psi} \mathbf{B}, \tag{5.94}$$

$$\mathbf{J}_{||} = h \frac{\partial p}{\partial \psi} \mathbf{B}. \tag{5.95}$$

By trivially equating the two expressions yields

$$B_\alpha = -B^2 B^\zeta h \sqrt{g}. \tag{5.96}$$

Considering the location at the outboard midplane as the beginning of the calculation, this expression becomes

$$B_\alpha = -B^2 B^\zeta h_o \sqrt{g}. \tag{5.97}$$

where h_o was calculated as described in Section 5.4.3.

As noted before, $\mathbf{B}=B_\Phi \hat{\mathbf{\Phi}}+B_Z \hat{\mathbf{Z}}$ and $\nabla\Psi=P_\psi \hat{\mathbf{R}}$ at the outboard midplane, so that B_α can be written as

$$B_\alpha = \mathbf{B}\cdot\mathbf{e}_\alpha = \left(B_\Phi \hat{\mathbf{O}} + B_Z \hat{\mathbf{Z}}\right)\sqrt{g}\left[P_\Psi \hat{\mathbf{R}} \times \left(\frac{Q_\zeta}{R}\hat{\mathbf{O}} + G_\zeta \hat{\mathbf{Z}}\right)\right]. \tag{5.98}$$

This can be simplified to

$$B_\alpha = P_\Psi \sqrt{g}\left(B_Z \frac{Q_\zeta}{R} - B_\Phi G_\zeta\right). \tag{5.99}$$

This can be combined with (5.97) to yield

$$-\frac{B^2 B^\zeta h_o}{P_\Psi} = B_Z \frac{Q_\zeta}{R} - B_\Phi G_\zeta. \tag{5.100}$$

Finally, this expression can be combined with (5.50) above to yield

$$\begin{bmatrix} \frac{B_\Phi}{R} & B_Z \\ \frac{B_Z}{R} & -B_\Phi \end{bmatrix} \begin{bmatrix} Q_\zeta \\ G_\zeta \end{bmatrix} = \begin{bmatrix} B^\zeta \\ -\frac{B^2 B^\zeta h_o}{P_\Psi} \end{bmatrix}. \tag{5.101}$$

In summary, once h_o is known by the numerical Pfirsch-Schlueter current calculation, (5.101) can be used to solved for Q_ξ and G_ξ. When that step is completed, Q_α and G_α can be solved for using (5.51) and (5.52). This completes the calculation of the initial conditions necessary to integrate forward the components of the three contravariant basis vectors.

5.4.6: Example Calculations of the Basis Vectors.

The QHS surface with near the mid-radius at the Φ=0 symmetry plane will be chosen to illustrate the features of this calculation. For comparison, the lab poloidal angle is plotted against the Hamada poloidal angle in the left of figure 5.11. The right frame of this figure shows the comparison between B_α and $-B^2h/2\pi$. These two quantities should be equal to each other at all points, according to expression (5.96). The B_α in this figure was calculated from the covariant basis vectors and the magnetic field vector (B_α=**B**·**e**$_\alpha$), while the value of h was calculated via the Nemov technique described in Section 5.4.3. There is excellent agreement between the two calculations, as anticipated

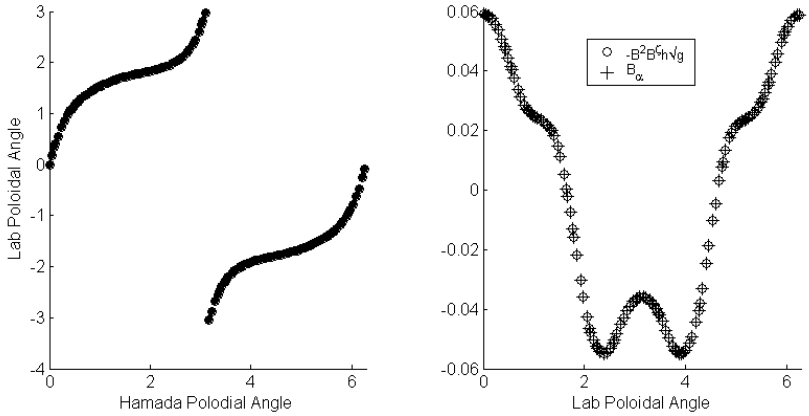

Figure 5.11: Comparison of lab and Hamada poloidal angles (left), and of the equality $B_\alpha=-B^2h/2\pi$ (right)

The basis vectors themselves are illustrated in figure 5.12, where all nine components are plotted against the Hamada poloidal angle, at the Φ=0 symmetry plane. The curves are all single valued, indicating the good convergence of the calculations. As examples of the

interpretation of this figure, note that both Q_ψ and G_ψ, corresponding to the Φ and Z components of $\nabla\psi$, are both zero at α=0 and α=π/2. Hence, $\nabla\psi$ points only in the R direction at the outboard midplane, as argued in Section 5.4.2. If this were an axisymmetric machine, then Q_ψ would be identically zero.

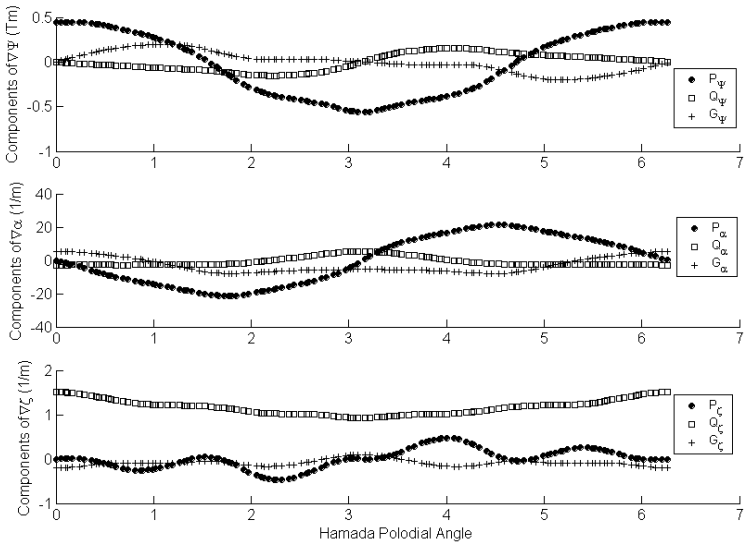

Figure 5.12: The components of the basis vectors plotted against the Hamada poloidal angle at the Φ=0 symmetry plane.

The basis vectors for the QHS configuration are plotted in figures 5.13 and 5.14. In these plots, the view is orthogonal to the flux surface, i.e. the plots are in the toroidal-poloidal plane. Figure 5.13 illustrates the basis vectors at the center flange between coils 1 and 2, where the low field side is on the outboard side of the torus. Figure 5.14 illustrates the basis vectors at the center flange between coils 5 and 6, where the high field side is on the outboard side of the torus. The direction of symmetry in the (n,m)=(4,1) component of the magnetic field is also shown. The direction of the magnetic field is also shown for reference; the plots are oriented so that the magnetic field always points directly to the right. It can be easily observed that these vectors satisfy the orthogonality conditions (for instance, $\mathbf{e}_\alpha \propto \nabla\psi \times \nabla\zeta$).

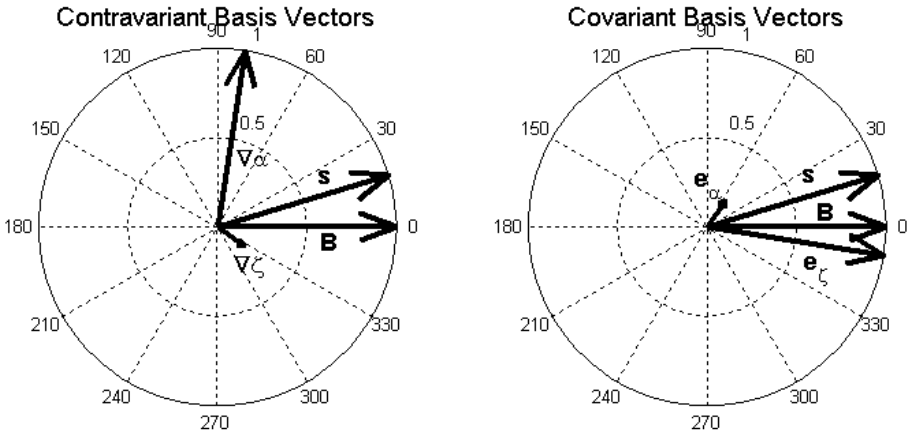

Figure 5.13: The contravariant and covariant basis vectors for the QHS case at the middle port between coils 1 and 2 (low field side), at r/a≈0.85.

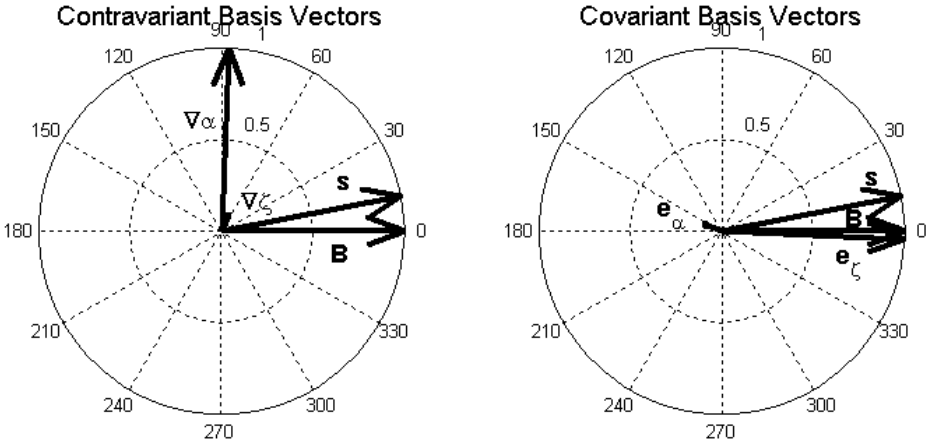

Figure 5.14: The contravariant and covariant basis vectors for the QHS case at the outboard port between coils 5 and 6 (high field side), at r/a≈0.9.

Note that the direction of the vector $\mathbf{e}_\alpha$ has a very different orientation with respect to the magnetic field at these two locations. This approximate reversal of the vector $\mathbf{e}_\alpha$ is physically significant. Recall from Section 5.4.4 that the **ExB** and diamagnetic flows are accompanied by compensating flows that maintain incompressibility. These Pfirsch-Schlueter flows are directly analogous to the Pfirsch-Schlueter current. The sum of all these flows can be summed to a single flow in the covariant poloidal direction, as in (5.91). The apparent reversal of the vector $\mathbf{e}_\alpha$ from high to low field sides of the machine represents the helical nature of the Pfirsch-Schueter current in HSX. When measured from the *outboard* of the machine, the Pfirsch-Schlueter current will

appear to reverse signs when measured near the boxport (the low field side and toroidal angle of zero) and near the joint flange (high field side, near toroidal angle of $\pi/4$).

The convergence of the flux surface averages is shown in figure 5.15, where the independent variable is the total toroidal angle integrated through. After some initial oscillation, the averages all settle at a value. This value is chosen by averaging the last half of the points, and that averaged value is shown as a thin line in the graph. These quantities are used as input to the damping rate calculations after proper conversion from mks to cgs units.

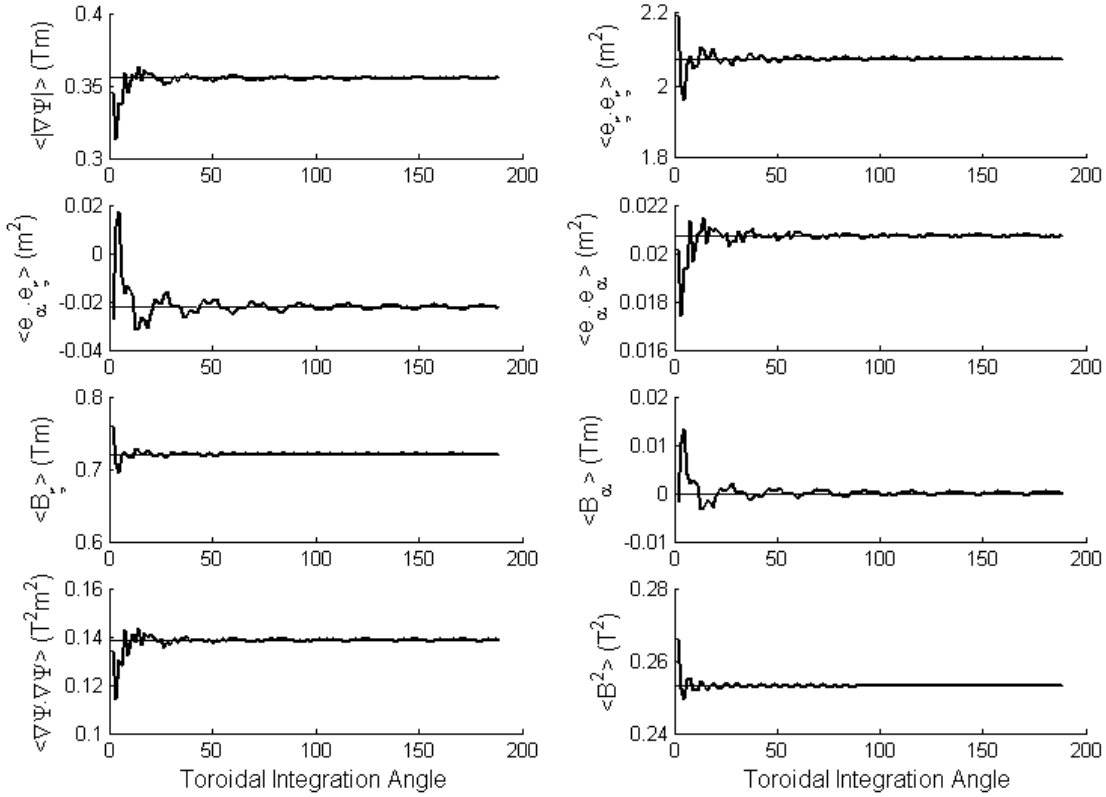

Figure 5.15: The convergence of the flux surface averaged quantities.

5.5: Comparisons between the Large Aspect Ratio Tokamak Approximation and Numerical Calculations for HSX.

Previous applications of neoclassical modeling[8] have used the basis vectors for a large aspect ratio tokamak. These have been calculated by Coronado and Trejo[9] for a circular cross section tokamak with magnetic field specified as

$$\mathbf{B} = \frac{B_o}{1+\varepsilon\cos(\theta)}\left(\Theta(r)\hat{\mathbf{e}} + \ddot{\mathbf{O}}\right), \tag{5.102}$$

where $\Theta=\varepsilon/q(r)$ and $\varepsilon=r/R_o$. Using volume as the flux label and defining the Hamada toroidal and poloidal angle to vary from 0 to 2π, the contravariant field components are given to lowest order in ε as

$$B^{\zeta} = B_o / R_o , \tag{5.103}$$

$$B^{\alpha} = \text{ł} B_o / R_o . \tag{5.104}$$

The flux surface quantities needed in the neoclassical modeling are given by:

$$\left\langle B^2 \right\rangle = \left\langle \mathbf{B}_T \cdot \mathbf{B} \right\rangle = \left\langle \mathbf{B}_T \cdot \mathbf{B}_T \right\rangle = B_o^2, \tag{5.105}$$

$$\left\langle \mathbf{B}_P \cdot \mathbf{B} \right\rangle = \left(\varepsilon B_o \text{ł}\right)^2, \tag{5.106}$$

$$\left\langle \mathbf{B}_P \cdot \mathbf{B}_P \right\rangle = \left(\varepsilon B_o \text{ł}\right)^2 \left(1 + 2q^2\right), \tag{5.107}$$

$$\left\langle B_{\zeta} \right\rangle = B_o R_o , \tag{5.108}$$

$$\left\langle B_{\alpha} \right\rangle = B_o r \varepsilon \text{ł} , \tag{5.109}$$

$$\sqrt{g} = 1 / 4\pi^2 , \tag{5.110}$$

These analytic approximations can be compared to the numerical calculations for the QHS configuration of HSX, shown in figure 5.16. The analytic expressions for $\langle B^2 \rangle$, $\langle \mathbf{B}\cdot\mathbf{B}_T \rangle$,

$\langle \mathbf{B}_P \cdot \mathbf{B}_P \rangle$, $\langle B_\zeta \rangle$ match the equivalent numerical parameter quite well. Note that the form of $\langle B_\zeta \rangle$ given in (5.108) is also the Boozer g number for a tokamak, a result which is generically true. The numerically calculated $\langle B_\zeta \rangle$ for HSX agrees precisely with g_B for HSX.

There are significant disagreements between the tokamak approximation and the numerical calculation in the terms which are proportional to $\langle B_\alpha \rangle$. It can be shown that $\langle B_\alpha \rangle$ is related to the toroidal current

$$\langle B_\alpha \rangle \propto \iint \mathbf{J} \cdot d\mathbf{A}_T \,. \tag{5.111}$$

Hence, this term is non-zero in a tokamak, but is exactly zero in a net current free stellarator like HSX (recall that the calculation is done for the vacuum field, and that pressure induced currents are expected to be small in the low-β plasmas in HSX). Other configurations of HSX (Mirror, Well), have similar levels of agreement and disagreement with the tokamak approximations.

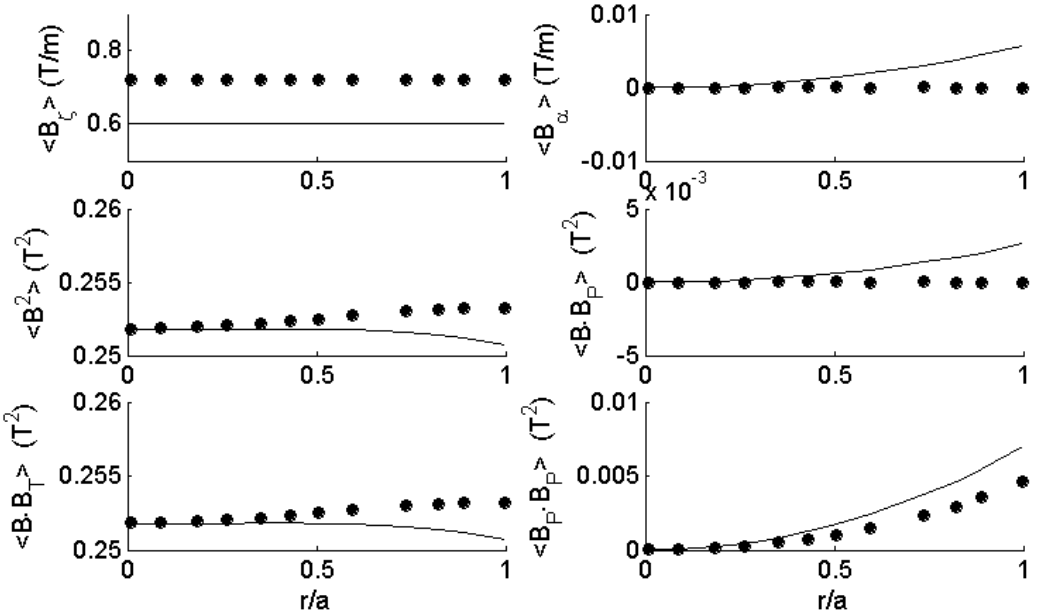

Figure 5.16: Comparison Between numerical and analytic calculations of the flux surface averages

5.6 Summary

The chapter has provided the details of how the Hamada coordinate system is constructed for the HSX stellarator. The method of calculating the Hamada spectrum was presented, and examples of the spectra in different configurations were presented. It was shown that the quasi-symmetry can be broken in two different ways. One way is by making large changes to the variation of |B| around the torus while leaving the field line trajectory largely unchanged; this is the symmetry breaking method in the Mirror configuration. A second means of breaking the symmetry involves the introduction of magnetic islands into the configuration. The changes in the surface shape in the vicinity of the magnetic islands can result in breaking of the quasi-symmetry.

A method of calculating the Hamada basis vectors for an arbitrary toroidal device has been presented. The method is based on integrating the basis vectors along a field line. To start this integration, it is necessary to know the initial conditions for the integration, i.e. the value of the basis vectors at some point in the machine. A method for calculating the basis vectors at the outboard midplane was presented, based upon numerical and analytic calculations of the Pfirsch-Schlueter current. Examples of the basis vector calculation were presented, including a comparison to the large aspect ratio tokamak basis vectors that have been used in neoclassical calculations in the past.

[1] W.D. D'haeseleer, W.N.G. Hitchon, J.D. Callen, and J.L. Shohet, *Flux Coordinates and Magnetic Field Structure*, (Springer, Berlin, 1991).

[2] G. Kuo-Petravic, A. H. Boozer, J.A. Rome, and R.H. Fowler, Journal of Computational Physics **51**, 261 (1983).

[3] J.N. Talmadge, Private Communication

[4] V.V.Nemov, Nuclear Fusion **28**, 1727 (1988).

[5] V.V. Nemov, Nuclear Fusion **30**, 927 (1990).

[6] K.C. Shaing and J.D. Callen, Phys. Fluids **26**, 3315 (1983).

[7] M. Coronado and H. Wobig, Phys. Fluids B **4**, 1294 (1992).

[8] M. Coronado and J.N. Talmadge, Phys. Fluids B **5**, 1200 (1993).

[9] M. Coronado and J. Galindo Trejo, Phys. Fluids B **2**, 530 (1990).